Atmos. Meas. Tech., 17, 3367–3375, 2024
https://doi.org/10.5194/amt-17-3367-2024

Atmospheric Measurement Techniques
Open Access
EGU

Innovative aerosol hygroscopic growth study from Mie–Raman–fluorescence lidar and microwave radiometer synergy

Robin Miri[1], Olivier Pujol[1], Qiaoyun Hu[1], Philippe Goloub[1], Igor Veselovskii[2,3], Thierry Podvin[1], and Fabrice Ducos[1]

[1]Univ. Lille, CNRS, UMR 8518 – LOA – Laboratoire d'Optique Atmosphérique, 59650 Villeneuve d'Ascq, France
[2]Prokhorov General Physics Institute of the Russian Academy of Sciences, Moscow 119991, Russia
[3]Cimel Electronique, 172 rue de Charonne, 75011 Paris, France

Correspondence: Robin Miri (robin.miri@univ-lille.frl)

Received: 10 January 2024 – Discussion started: 15 January 2024
Revised: 5 April 2024 – Accepted: 15 April 2024 – Published: 3 June 2024

Abstract. This study focuses on the characterization of aerosol hygroscopicity using remote sensing techniques. We employ a Mie–Raman–fluorescence lidar (Lille Lidar for Atmospheric Study, LILAS), developed at the ATOLL platform, Laboratoire d'Optique Atmosphérique, Lille, France, in combination with the RPG-HATPRO-G5 microwave radiometer to enable continuous aerosol and water vapor monitoring. We identify hygroscopic growth cases when an aerosol layer exhibits an increase in both aerosol backscattering coefficient and relative humidity. By examining the fluorescence backscattering coefficient, which remains unaffected by the presence of water vapor, the potential temperature, and the absolute humidity, we verify the homogeneity of the aerosol layer. Consequently, the change in the backscattering coefficient is solely attributed to water uptake. The Hänel theory is employed to describe the evolution of the backscattering coefficient with relative humidity and introduces a hygroscopic coefficient, γ, which depends on the aerosol type. The particularity of this method revolves around the use of the fluorescence which is employed to take into account and correct the aerosol concentration variations in the layer. Case studies conducted on 29 July and 9 March 2021 examine, respectively, an urban and a smoke aerosol layer. For the urban case, γ is estimated as 0.47 ± 0.03 at 532 nm; as for the smoke case, the estimation of γ is 0.5 ± 0.3. These values align with those reported in the literature for urban and smoke particles. Our findings highlight the efficiency of the Mie–Raman–fluorescence lidar and microwave radiometer synergy in characterizing aerosol hygroscopicity. The results contribute to advance our understanding of atmospheric processes, aerosol–cloud interactions, and climate modeling.

1 Introduction

Aerosols play a crucial role in our understanding of climate dynamics. Their impact on the radiation budget is classified into direct and semi-direct effects (Hansen et al., 1997; Thorsen et al., 2020), with additional contributions arising from aerosol–cloud interactions, commonly known as indirect effects. Certain aerosols can act as cloud condensation nuclei (CCN) or ice nucleating particle (INP), altering cloud properties including albedo and lifetime (Twomey and Warner, 1967). These complex processes remain significant challenges in the interpretation of the Earth energy balance. To advance our comprehension of aerosol–cloud interactions is crucial for improving climate models and accurately accounting for their influence on the energy balance of our planet. A key process in the understanding of these interactions is hygroscopic growth, which consists in aerosol uptake of water vapor in high relative humidity (RH) conditions, resulting in changes in size and, in some cases, chemical composition (Hänel, 1976). Hygroscopic growth efficiency varies depending on the aerosol type, with hydrophobic aerosols like dust and hydrophilic aerosols like marine particles (Chen et al., 2019, 2020). This variability is linked to their potential as CCN and INP, highlighting the importance of under-

standing the hygroscopic properties of aerosols (Dusek et al., 2006).

Hygroscopic growth properties of aerosols can be effectively investigated using a range of instruments. Traditionally, humidified nephelometers and spectrometers have been widely used to study aerosol hygroscopicity (Covert et al., 1972; Burgos et al., 2019). However, active remote sensing systems have tended to appear more advantageous since the last decade, as they allow us to measure with high vertical and temporal resolution without interfering with the observed system. Lidars, in particular, have gained prominence in remotely studying these properties (Feingold and Morley, 2003; Fernández et al., 2015; Granados-Muñoz et al., 2015; Zieger et al., 2015; Navas-Guzmán et al., 2019; Dawson et al., 2020; Düsing et al., 2021; Sicard et al., 2022, etc.) and offer several advantages compared to other methods. In particular, lidars provide high vertical and temporal resolution, allowing for detailed analysis of aerosol characteristics. Moreover, lidars offer the unique capability of simultaneously measuring aerosol properties and water vapor mixing ratio using a single instrument. At the Laboratoire d'Optique Atmosphérique (LOA) in Lille, France, the ATOLL platform (ATmospheric Observations in LiLLe) features a Mie–Raman–fluorescence lidar (Lille Lidar for Atmospheric Study, LILAS) employed in the frame of EARLINET/ACTRIS-FR (European Aerosol Research Lidar Network/Aerosols, Clouds, and Trace Gases Research Infrastructure – France). This multiwavelength lidar system measures elastic, depolarized, and Raman signals, providing comprehensive information on aerosol properties and water vapor. Additionally, LILAS captures aerosol fluorescence signal at 466 nm, which is triggered by the lidar UV wavelength at 355 nm. The fluorescence signal possesses distinctive characteristics that contribute to its utility in aerosol studies. Its intensity correlates with aerosol concentration and type, with biological aerosols like pollen or biomass burning smoke exhibiting higher fluorescence, while pure dust or urban aerosols demonstrate lower fluorescence. Furthermore, the fluorescence signal at 466 nm does not arise from pure water, enabling the extraction of aerosol-specific information without the influence of water vapor, which proves to be essential in studying aerosol hygroscopic growth (Veselovskii et al., 2020). In combination with an RPG-HATPRO-G5 microwave radiometer, also part of the ATOLL platform, it is possible to monitor both aerosol characteristics and water vapor, allowing us to study aerosol hygroscopicity.

The first part of this paper introduces the instruments and outlines a novel method for the study of aerosol hygroscopic growth using LILAS measurements. Following the instrument and method description, case studies are presented to demonstrate the efficiency and potential of the proposed approach. These case studies illustrate the practical implementation and feasibility of this innovative methodology, highlighting the added value brought by aerosol fluorescence measurement in offering valuable insights into the hygroscopic growth characteristics of these aerosols. Finally, the paper concludes with a summary of the findings and offers comments on the obtained results. The conclusions will also discuss the potential further advancements and applications of the developed method, emphasizing its importance in enhancing our understanding of hygroscopic growth phenomena and its broader implications for atmospheric research.

2 Instrumentation and methodology

2.1 Experimental setup and data treatment

All the measurements presented in this paper were performed at the ATOLL platform in Lille (50.611° N, 3.138° E). The first instrument used in this study is the lidar LILAS. Its emission component consists of a tripled Nd:YAG laser operating at a repetition rate of 20 Hz, with a pulse energy of 70 mJ at 355 nm. The lidar system is configured in the $3\beta + 2\alpha + 3\delta$ arrangement, meaning that it measures the elastic backscatter coefficient at three wavelengths (355, 532, and 1064 nm); it also measures the extinction at 355 and 532 nm, as well as the volume depolarization ratios for these wavelengths. This instrument also includes an additional channel for aerosol fluorescence detection, featuring a dedicated interference filter centered at 466 nm with a width of 44 nm. For this study, the aerosol elastic backscatter coefficients (β) and the particulate linear depolarization ratio (PLDR) were computed at 532 nm from a Mie–Raman observation (Ansmann et al., 1992), due to the high signal-to-noise ratio at this wavelength in comparison with the two others. Furthermore, the detection part of the lidar includes a channel specifically designed to measure the vibrational–rotational Raman scattering of water at 408 nm, allowing for the retrieval of water vapor mixing ratio profiles (Ansmann et al., 1992; Whiteman et al., 1992). The obtained profiles were acquired during nighttime only and averaged over a period of 60 min. General details about the system can be found in Hu et al. (2018) and Veselovskii et al. (2020).

The proximity of the ATOLL platform to the airport prohibits the use of radiosounding. This poses a challenge for the inversion of water vapor using the LILAS lidar, as the computation of the instrumental constant requires a reference. Moreover, radiosoundings traditionally provide temperature profiles which are crucial for calculating RH but are difficult to obtain otherwise.

The second instrument used in this study is the RPG-HATPRO-G5 microwave radiometer, developed by RPG Radiometer Physics GmbH and present at the ATOLL platform, which provides integrated information like integrated water vapor content (IWV) or liquid water content (LWC) but also uses an integrated neural network model to retrieve atmospheric profiles of temperature, humidity, and liquid water. In situ sensors allow for ground level measurement of temper-

ature, humidity, and pressure. Finally, an infrared radiometer extension allows us to detect cloud base height and ice clouds. Data are acquired at high temporal resolution (every 10 min), and profiles range from the ground to 10 km (Louf et al., 2015).

This instrument has been considered to compensate for the lack of radiosounding measurement at the ATOLL platform for the calibration of the lidar water vapor measurement. Unfortunately, after considering using the radiometer humidity and temperature profiles for the lidar calibration, these ones turned out to be insufficiently accurate.

Consequently, temperature profiles from the ERA5 reanalysis database were also collected, and the IWV measurement of the radiometer has been used to calibrate the lidar.

In order to compute the instrumental constant necessary for the lidar water vapor calibration, the radiometer IWV has been compared to the integral of absolute humidity (AH) between the ground and 6 km height (above which humidity is negligible), as derived from the lidar-measured water vapor mixing ratio and the ERA5 temperature. Following the calibration procedure described in Foth et al. (2015), the calibration constant of the instrument is determined as the ratio between IWV and the integral value. The calibrated water vapor mixing ratio can be computed with

$$\mathrm{x}_{\mathrm{H_2O}}(h) = \mathrm{x}'_{\mathrm{H_2O}}(h)\mathrm{IWV}\left[\int_0^{z_{\max}} \mathrm{x}'_{\mathrm{H_2O}}(h)\frac{P(h)}{R_{\mathrm{a}}T(h)}\mathrm{d}h\right]^{-1}, \quad (1)$$

where h is the height, $\mathrm{x}_{\mathrm{H_2O}}(h)$ and $\mathrm{x}'_{\mathrm{H_2O}}(h)$ are the calibrated and not-calibrated water vapor mixing ratios, respectively, $z_{\max}$ is equal to 6 km, P is the atmospheric pressure estimated with the hydrostatic approximation, R_{a} is the air perfect gas constant, and T is the temperature (all given in the International System of units). The calibration has been exclusively conducted under clear-sky conditions and taking into account the signal-to-noise ratio of the lidar's water vapor mixing ratio; if the signal-to-noise ratio on the profile is lower than 3, then the calibration constant is not computed. This threshold has been determined to ensure both data quality and a sufficient number of calibration constant computations. An interpolation has then been performed to estimate the calibration constants of cloudy and noisy situations.

2.2 Hygroscopic growth identification and study

In order to identify and analyze hygroscopic growth cases, a widely used method consists of searching for a homogeneous aerosol layer that spans either in time or altitude. When RH and elastic backscatter coefficient both increase, or decrease, it serves as a key indicator of hygroscopic growth. In the case of a homogeneous aerosol layer, the elastic backscatter coefficient evolution can then be attributed only to hygroscopic growth. This approach enables us to relate the elastic backscatter coefficient and RH, characterizing the hygroscopic properties of the considered aerosol particles.

The verification of the homogeneous nature of the considered aerosol layer is generally performed by investigating two key variables, absolute humidity, and potential temperature. Absolute humidity is investigated in order to identify any changes in the air mass that would lead to a change in the absolute humidity. A constant or decreasing potential temperature means that strong mixing is occurring within the layer, thus supporting the idea that the layer is homogeneous (Granados-Muñoz et al., 2015; Navas-Guzmán et al., 2019; Sicard et al., 2022).

The focus of this paper deals with the valuable insights provided by β_{fluo}. As stated in Veselovskii et al. (2020), a fluorescence signal emitted by aerosols at around 466 nm is not expected to be impacted by the presence of water, as pure water does not fluoresce. Therefore, by assuming that hygroscopic growth does not impact aerosol fluorescence and that the aerosol mixing state remains the same in the considered layer, β_{fluo} becomes a reliable proxy for monitoring the concentration of dry material within the aerosol layer. Under the hypothesis of a constant aerosol mixture and chemical composition in the layer, normalizing β_{532} by β_{fluo} enables the study of hygroscopic growth properties while also accounting for any possible changes in aerosol concentration within the layer.

Once the hygroscopic growth case has been identified, it becomes possible to examine the correlations between aerosol optical properties and RH. In this paper, particular attention has been given in the investigation of β_{532}. In order to explore this correlation efficiently, the Hänel parameterization has been used to express the changes in β_{532} as a function of RH. It introduces a parameter γ, known as the hygroscopic growth factor, which depends on the wavelength and the type of aerosol (Hänel, 1976). The Hänel parameterization is represented by

$$\frac{\beta_{532}(\mathrm{RH})}{\beta_{532}(\mathrm{RH_{ref}})} = \left(\frac{100-\mathrm{RH}}{100-\mathrm{RH_{ref}}}\right)^{-\gamma}, \quad (2)$$

where $\mathrm{RH_{ref}}$ is the reference relative humidity. From this parameterization, it is possible to use β_{fluo} to account for aerosol concentration changes within the layer by normalizing β_{532}, so that

$$\frac{\beta_{532}(\mathrm{RH})}{\beta_{532}(\mathrm{RH_{ref}})}\frac{\beta_{\mathrm{fluo}}(\mathrm{RH_{ref}})}{\beta_{\mathrm{fluo}}(\mathrm{RH})} = \left(\frac{100-\mathrm{RH}}{100-\mathrm{RH_{ref}}}\right)^{-\gamma}. \quad (3)$$

We obtain an accurate estimation of the hygroscopic parameter γ by fitting the variation of β_{532} with respect to RH to the function as follows:

$$\beta_{532}(\mathrm{RH}) = \beta_{532}(\mathrm{RH_{min}})\frac{\beta_{\mathrm{fluo}}(\mathrm{RH})}{\beta_{\mathrm{fluo}}(\mathrm{RH_{min}})}\left(\frac{100-\mathrm{RH}}{100-\mathrm{RH_{min}}}\right)^{-\gamma}, \quad (4)$$

where $\mathrm{RH_{min}}$ represents the minimum relative humidity observed within the analyzed aerosol layer. Subsequently, the estimations of γ values can be compared to hygroscopic growth parameter estimations from previous studies, the type

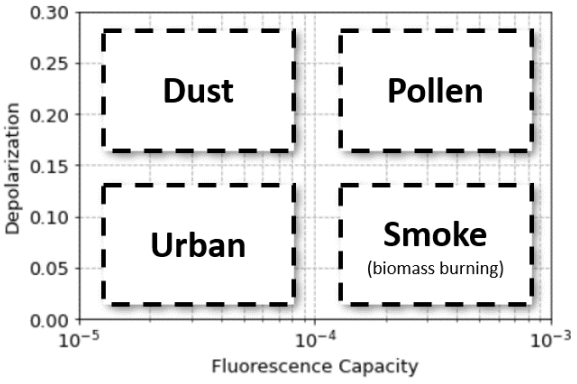

Figure 1. Schematic empirical aerosol typing repartition in function of the depolarization (PLDR) and fluorescence capacity (adapted from Veselovskii et al., 2022).

of the aerosol can be estimated from the optical properties, mainly its fluorescence capacity (the ratio between the fluorescence and elastic backscatter coefficients), and PLDR (Veselovskii et al., 2022) as shown Fig. 1. This comparative analysis offers valuable insights into how the hygroscopic growth of aerosols relates to their specific compositions and sources, contributing to a deeper understanding of aerosol behavior in changing environmental conditions.

3 Results and discussions

In order to experiment the potential of the hygroscopic growth study approach, this method has been tested on two potential hygroscopic growth cases, with the first occurring during 29 July 2021, averaged from 22:00 to 23:00 UTC, and the second occurring during 9 March 2021, averaged from 21:00 to 22:00 UTC.

3.1 Hygroscopic growth study during the event on 29 July 2021 from 22:00 to 23:00 UTC

Figure 2 shows the profiles of the different measurements for the case study of 29 July 2021. In this particular scenario, both the water vapor mixing ratio and potential temperature exhibit relative stability, which are the two criteria commonly used to assess that the considered aerosol layer, are homogeneous (Granados-Muñoz et al., 2015; Navas-Guzmán et al., 2019; Sicard et al., 2022). Even though the potential temperature is derived from ERA5 reanalysis temperature profiles rather than direct measurements, this still provides a strong indication of the aerosol layer homogeneity. Moreover, β_{fluo} does not show strong variations within the defined region (the standard deviation of β_{fluo} in the considered layer is about 10 % of the average), further supporting this conclusion.

Conversely, there is an increase in both β_{532} and RH, suggesting a potential case of hygroscopic growth. RH rises from 74 % to 96 %, which is a significant growth and strongly supports the hypothesis that hygroscopic growth occurs. Last, depolarization is not expected to decrease as it is already low, even if hygroscopic growth occurs.

Finally, it is possible to estimate the aerosol type of the considered layer by looking at its optical properties. Figure 3 shows the scatterplot of the PLDR at 532 nm and the fluorescence capacity, which is here the ratio between β_{fluo} and β_{532}. The considered aerosol layer exhibits low PLDR, as well as low fluorescence capacity characteristics, that allow it to be identified as an urban aerosol layer.

Figure 4 presents the outcomes of the fitting process for the relationship between β_{532} and RH using the Hänel parameterization. These results indicate a good fit to the Hänel parameterization in this particular case, as evidenced by the determination coefficient being close to 1 ($R^2 = 0.91$). However, the estimated value of γ, which is expected to fall between 0.3 and 0.5 for a case of urban particles (Navas-Guzmán et al., 2019), is equal to 0.31 in this instance, which is very close to the lower limit for this type of aerosol. It also comes along with a slight divergence between the fit and the data, especially at high RH.

Several factors may contribute to the deterioration of the results and explain the low value of γ. First, it is possible that, in this case, there is merely no significant hygroscopic growth occurring for this particular type of aerosol within the observed range of RH. However, given the substantial RH variation, starting at 74 % and reaching up to 96 %, this hypothesis becomes less plausible.

Second, it is possible that the main assumption on which this parameterization lies, i.e., constant aerosol concentration within the observed layer, may not hold true. Even with stable potential temperature and water vapor mixing ratio, there is a possibility that the aerosol concentration varies within the designated area, especially considering that potential temperature is derived from ERA5 reanalysis profiles and not directly measured. This potential aerosol concentration variation could potentially account for the low estimation of the hygroscopic growth factor.

In order to investigate this, we can assume that aerosol mixing remains constant within the study area and that β_{fluo} varies solely with changes in aerosol concentration. In doing so, it becomes possible to normalize β_{532} based on variations in aerosol concentration according to

$$\overline{\beta_{532}}\,(\text{RH}) = \beta_{532}\,(\text{RH})\,\frac{\beta_{\text{fluo}}\,(\text{RH}_{\text{min}})}{\beta_{\text{fluo}}(\text{RH})}\,. \tag{5}$$

Here, $\overline{\beta_{532}}(\text{RH})$ is the normalized elastic backscatter coefficient, and $\beta_{\text{fluo}}\,(\text{RH}_{\text{min}})$ is β_{fluo} at the minimum value of RH in the studied area.

It is now possible to apply the Hänel parameterization to $\overline{\beta_{532}}$ instead of β_{532} in order to take into account the aerosol concentration variations within the layer and assess whether this normalization yields improved results.

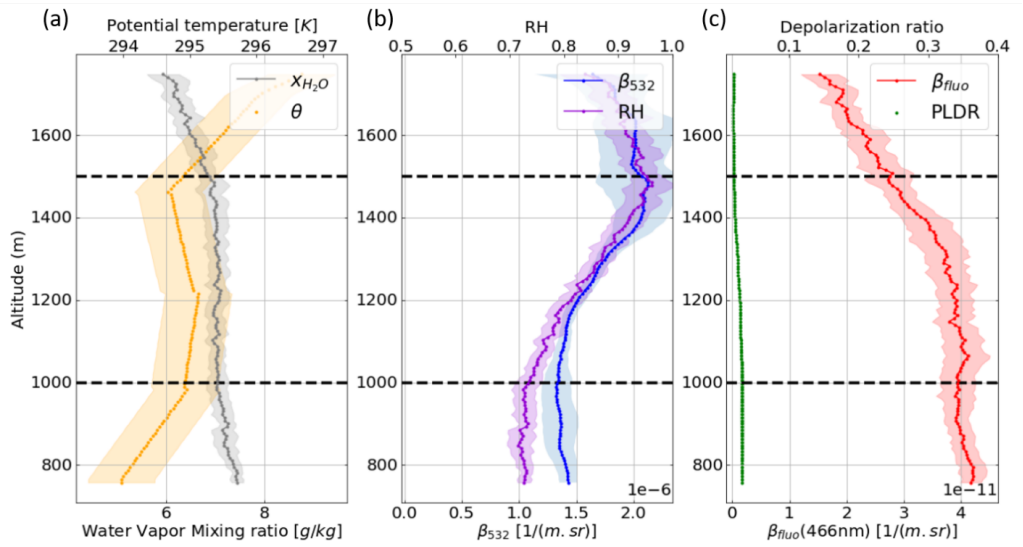

Figure 2. Profile of retrieved optical properties as a function of altitude above ground level. **(a)** Water vapor mixing ratio [$g\,kg^{-1}$] and potential temperature [K], **(b)** elastic backscatter coefficient at 532 nm [$m^{(-1)}\,sr^{(-1)}$] and RH, and **(c)** fluorescence backscatter coefficient at 466 nm [$m^{(-1)}\,sr^{(-1)}$] and PLDR at 532 nm on 29 July 2021 from 22:00 to 23:00 UTC. The dashed black lines identify the area where hygroscopic growth is expected to occur.

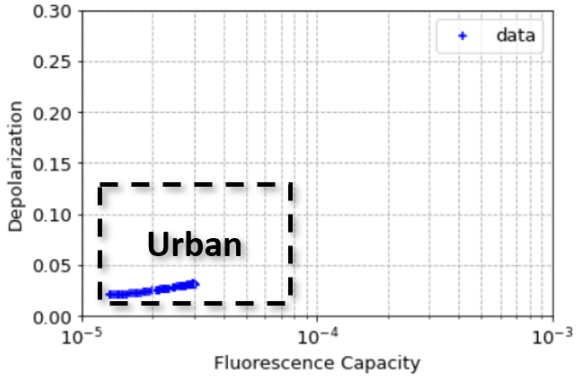

Figure 3. Fluorescence capacity (β_{fluo}/β_{532}) and PLDR at 532 nm between 1000 and 1500 m above ground level on 29 July 2021 from 22:00 to 23:00 UTC, characteristic of an urban aerosol layer.

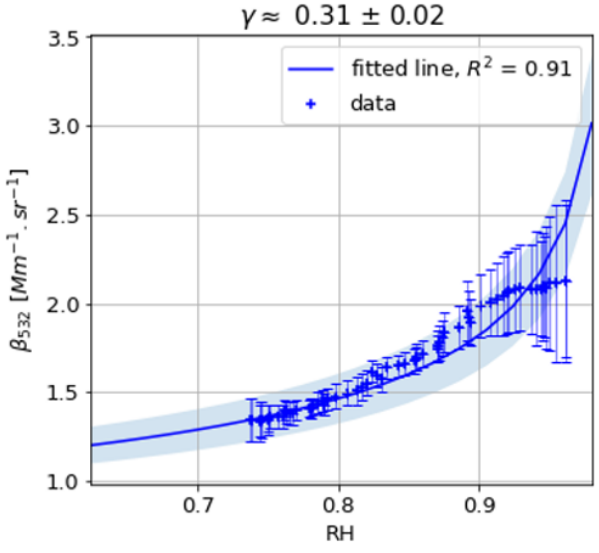

Figure 4. Evolution of the elastic backscatter coefficient at 532 nm as a function of RH on 29 July 2021 from 22:00 to 23:00 UTC between 1000 and 1500 m above ground level and the results of the fit to the Hänel parameterization.

The relationship between $\overline{\beta_{532}}$ and RH, along with its fit to the Hänel parameterization presented in Fig. 5, demonstrates a significantly improved fit to the Hänel parameterization, with a notably higher determination coefficient ($R^2 = 0.98$ instead of 0.91). Furthermore, the estimation of γ is found to be equal to 0.47 ± 0.03, falling precisely within the range of estimations conducted at 532 nm by previous studies (Navas-Guzmán et al., 2019; Sicard et al., 2022). These findings support the hypothesis that aerosol concentration varies within the aerosol layer and that such fluctuations are traceable through β_{fluo}, corroborating the efficiency of the presented approach for investigating hygroscopic growth phenomena.

3.2 Hygroscopic growth study during the event on 9 March from 21:00 to 22:00 UTC

Another case study can be presented to further support the validity of this approach. It is the case occurring on 9 March 2021 and averaged between 21:00 and 22:00 UTC.

Figure 6 shows the profiles of the different measurements for the case study on 9 March 2021. In this situation, both

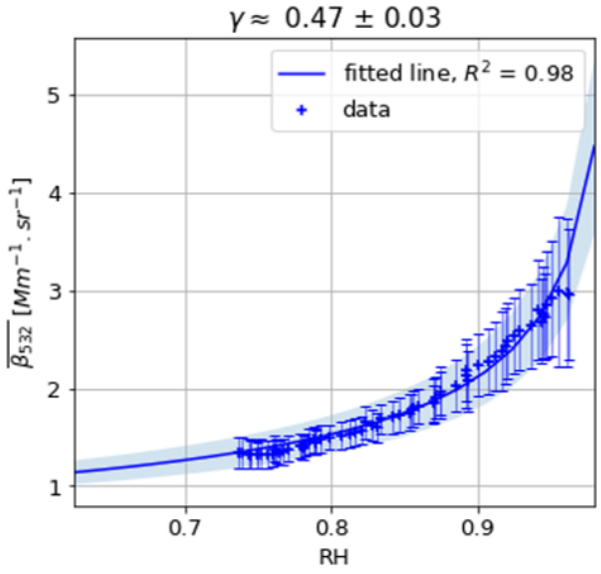

Figure 5. Evolution of the normalized elastic backscatter coefficient at 532 nm (normalized with fluorescence backscatter coefficient) as a function of RH on 29 July 2021 from 22:00 to 23:00 UTC between 1000 and 1500 m above ground level and the results of the fit to the Hänel parameterization.

the water vapor mixing ratio and the potential temperature are relatively stable in the layer (potential temperature variations remain under 2 K, and the water vapor mixing ratio variations remain under 1 g kg^{-1}), indicating a good mixing in the considered layer. An increase in both RH and β_{532} can also be noticed. On the other hand, there are fluctuations of β_{fluo}, mostly in the lower part of the layer, and the PLDR remains stable, but once again, given its already low value, it is not expected to decrease with hygroscopic growth. These elements together indicate that a hygroscopic growth scenario is most likely to occur in this layer.

The aerosol type can be investigated once again by looking at the fluorescence capacity and the PLDR. Both are represented Fig. 7 and show characteristics indicating that the aerosol layer comes from biomass burning smoke with low PLDR and strong fluorescence. Something worth noticing, however, is the low value of the fluorescence capacity. Indeed, the fluorescence capacity is the ratio between fluorescence backscatter coefficient and elastic backscatter coefficient. While the first is expected to remain stable with hygroscopic growth, the second increases in a high-humidity condition, consequently decreasing the fluorescence capacity and potentially leading to misclassification as indicated in Veselovskii et al. (2020). In this case, however, it is still possible to identify the biomass burning smoke aerosol layer.

The results of the fit to the Hänel parameterization on both β_{532} and $\overline{\beta_{532}}$ (shown in Fig. 8) indicate a significant improvement brought by the normalization with the fluorescence. Without this process, the fit to the Hänel parameterization is extremely poor, with $R^2 = -0.06$. Furthermore, the estimation of the hygroscopic growth parameter is much lower than expected ($\gamma = 0.1 \pm 0.3$), while the value is expected to fall around 0.5 at 532 nm for smoke aerosols according to Gomez et al. (2018). On the other hand, using the information given by the fluorescence to normalize the elastic backscatter coefficient, it is possible to obtain a much better fit to the Hänel parameterization, with $R^2 = 0.93$ and a better estimation of the hygroscopic growth parameter, with $\gamma = 0.5 \pm 0.3$ falling in the expected range for smoke aerosols. These findings suggest that it is indeed possible to use β_{fluo} to correct the variation in the aerosol concentration within the aerosol layer to study hygroscopic growth. The only drawback of this case lies in its high uncertainty.

An explanation for this high uncertainty could be instrumental noise, the span of RH covered being narrower than the first presented case (RH varying from 77.8 % to 87.6 %), or even the atmospheric variability being more important in this situation. Nevertheless, the point demonstrated in this analysis relies in the utility of the fluorescence correction for the hygroscopic factor estimation which is well emphasized here.

The influence of a shift in RH on γ has also been examined. For the case on 9 March 2021, when a bias of minus 0.1 is manually introduced to the RH, the corresponding γ estimation becomes 0.82, while a positive bias of 0.1 in RH results in a γ value of 0.23. The estimation of RH is based on both measurement from LILAS and the radiometer but also on ERA5 reanalysis data, which heavily rely on computational models. While this estimation provides valuable insights, it inherently introduces a level of uncertainty to the results. It is anticipated that the uncertainty associated with this estimation falls within the range of 10 %. The estimation of γ and the conclusions drawn from this estimation should then be considered with caution. Future studies might focus on refining the methods used for RH estimation, aiming at minimizing this inherent uncertainty and enhancing the accuracy of these findings. However, even if a shift in RH introduces high variability in γ, the determination coefficient R^2 remains almost unchanged ($R^2 = 0.92$ when RH is decreased by 0.1 and $R^2 = 0.91$ for a 0.1 increase), meaning that the conclusions drawn on the use of the fluorescence correction are still valid in spite of the uncertainty in RH.

4 Conclusion

In this article, we have examined the possibility of using LILAS data for aerosol hygroscopic growth studies. The calibration of LILAS's water vapor channel has been addressed using thermodynamic data from the RPG-HATPRO-G5 microwave radiometer and temperature data from ERA5 reanalysis. A new approach to analyze aerosol hygroscopicity, relying on the fluorescence profiles measured by LILAS, has been developed and tested on two situations.

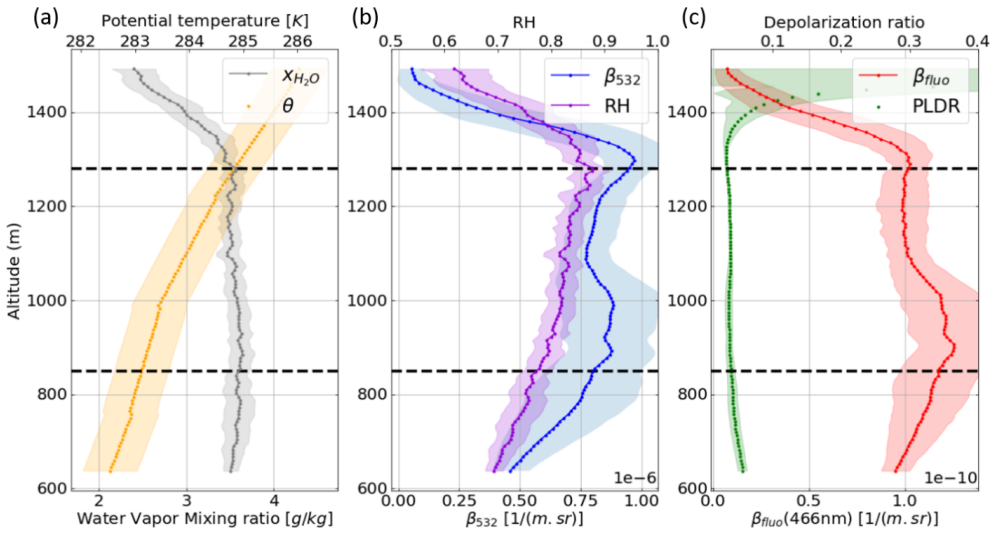

Figure 6. Profile of retrieved optical properties as a function of altitude above ground level. **(a)** Water vapor mixing ratio [g kg^{-1}] and potential temperature [K], **(b)** elastic backscatter coefficient at 532 nm [1 m$^{(-1)}$ sr$^{(-1)}$] and RH, **(c)** fluorescence backscatter coefficient at 466 nm [1 m$^{(-1)}$ sr$^{(-1)}$] and PLDR at 532 nm on 9 March 2021 from 21:00 to 22:00 UTC. The dashed black lines identify the area where hygroscopic growth is expected to occur.

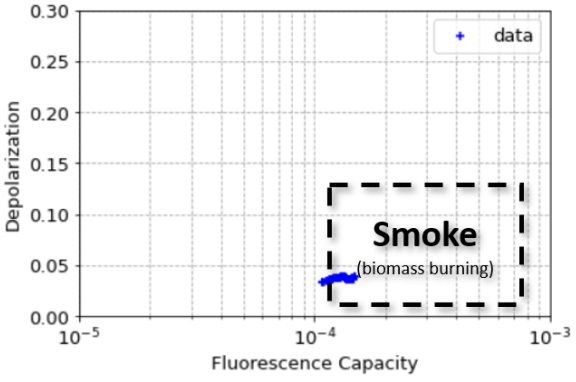

Figure 7. Fluorescence capacity ($\beta_{\text{fluo}}/\beta_{532}$) and PLDR at 532 nm between 850 and 1280 m above ground level on 9 March 2021 from 21:00 to 22:00 UTC, characteristic of a biomass burning smoke aerosol layer.

The unique feature of the method presented in this article hinges on its use of the fluorescence backscatter coefficient. This coefficient serves as a weighting factor in tracking the evolution of aerosol concentration within the aerosol layer. Consequently, it leads to a significantly improved representation of the hygroscopic state evolution of the aerosols, thereby enhancing the characterization of the Hänel hygroscopic coefficient, γ. To validate this approach, evaluations were performed on two cases from July and March 2021, yielding promising results and highlighting the value brought by the fluorescence backscatter coefficient measurement with the lidar. In the first case, an estimation of γ of 0.47 ± 0.03 with the fluorescence correction fell in the expected range of the hygroscopic growth parameter for urban aerosols at 532 nm. In the second case, the estimation of γ is 0.5 ± 0.3, which, despite the higher uncertainty, is in the expected value for smoke particles at 532 nm and, most importantly, is a great improvement compared to the estimation carried on without the fluorescence correction.

In order to further increase the accuracy of our results, this method could be applied to a site featuring both fluorescence lidar measurement, as well as radiosoundings, in order to better estimate RH, a variable that significantly influences γ estimation and which is really complicated to estimate accurately otherwise. Based on the presented approach, values of γ can be calculated for various types of aerosols, and the assessment of the relationship between γ and aerosol optical properties like PLDR or fluorescence capacity can be considered. These relationships are expected to provide valuable insights for modeling interactions between aerosols and water vapor, serving as an initial step in studying aerosol–cloud interactions (Dusek et al., 2006; Petters and Kreideweis, 2007).

However, a current limitation of the present work arises in the identification of hygroscopic growth cases (which is done manually). Future efforts could focus on automatically identifying hygroscopic growth cases using lidar measurements, simplifying the study of γ dependency with aerosol parameters in a large number of situations (Gysel et al., 2007). From this perspective, an automatic classification method is also currently being developed, using a clustering approach, in order to automatically classify aerosol layers based on their optical properties, as well as thermodynamic parameters, accounting for humidity impact on the fluorescence capacity, as illustrated in the analysis of Fig. 7.

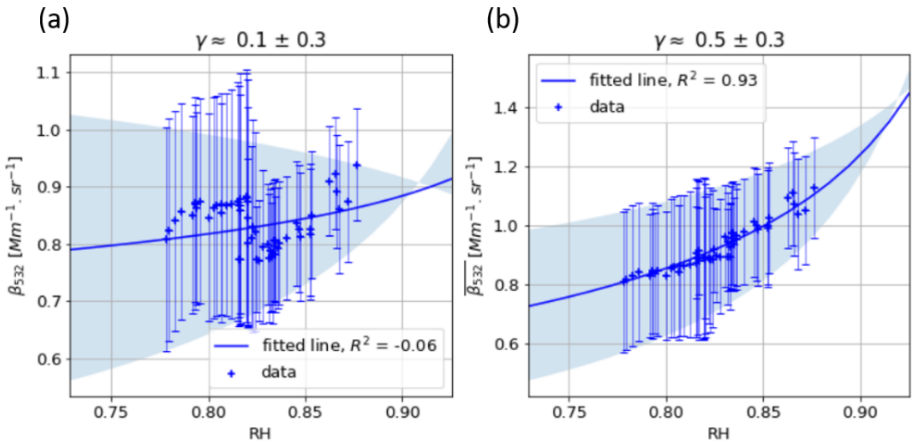

Figure 8. Evolution of the elastic backscatter coefficient at 532 nm **(a)** without normalization and **(b)** with normalization with the fluorescence backscatter coefficient and as a function of RH on 9 March 2021 from 21:00 to 22:00 UTC between 850 and 1280 m above ground level and the results of the fit to the Hänel parameterization.

Furthermore, the hygroscopic growth study will be adapted and improved for the LIFE lidar (laser-induced fluorescence explorer), which is anticipated to be operational by 2024. This upcoming lidar system is set to have more power and include additional fluorescence channels, thereby increasing the amount of information available, which will significantly enhance the retrieval performance.

Code and data availability. Data and code will be made available upon the request to the corresponding author.

Author contributions. RM analyzed the LILAS data, prepared the figures, and wrote the manuscript. PG, OP, IV, and QH supervised the work and contributed to the writing of the manuscript. PG, QH, IV, and TP designed, conceived, and ran the LILAS instrument. FD and QH developed and supported LILAS algorithms. OP is in charge of the RPG-HATPRO-G5 microwave radiometer.

Competing interests. The contact author has declared that none of the authors has any competing interests.

Disclaimer. Publisher's note: Copernicus Publications remains neutral with regard to jurisdictional claims made in the text, published maps, institutional affiliations, or any other geographical representation in this paper. While Copernicus Publications makes every effort to include appropriate place names, the final responsibility lies with the authors.

Acknowledgements. We acknowledge the CaPPA project funded by the ANR through the PIA (under contract no. ANR-11-LABX-0005-01). The authors thank the Région Hauts-de-France, the Ministère de l'Enseignement Supérieur et de la Recherche, and the European Fund for Regional Economic Development for their financial support to the CPER CLIMIBIO and ECRIN programs. The contribution from Qiaoyun Hu has been supported by Agence Nationale de Recherche ANR (grant no. ANR-21-ESRE-0013) through the OBS4CLIM project.

ChatGPT has been employed for drafting purposes in this document.

Financial support. This research has been supported by the Agence Nationale de la Recherche (grant nos. ANR-11-LABX-0005-01 and ANR-21-ESRE-0013).

Review statement. This paper was edited by Ulla Wandinger and reviewed by two anonymous referees.

References

Ansmann, A., Riebesell, M., Wandinger, U., Weitkamp, C., Voss, E., Lahmann, W., and Michaelis, W.: Combined raman elastic-backscatter LIDAR for vertical profiling of moisture, aerosol extinction, backscatter, and LIDAR ratio, Appl. Phys. B-Lasers O., 55, 18–28, https://doi.org/10.1007/BF00348608, 1992.

Burgos, M. A., Andrews, E., Titos, G., Alados-Arboledas, L., Baltensperger, U., Day, D., Jefferson, A., Kalivitis, N., Mihalopoulos, N., Sherman, J., Sun, J., Weingartner, E., and Zieger, P.: A global view on the effect of water uptake on aerosol particle light scattering, Sci. Data, 6, 157, https://doi.org/10.1038/s41597-019-0158-7, 2019.

Chen, J., Li, Z., Lv, M., Wang, Y., Wang, W., Zhang, Y., Wang, H., Yan, X., Sun, Y., and Cribb, M.: Aerosol hygroscopic growth, contributing factors, and impact on haze events in a severely polluted region in northern China, Atmos. Chem. Phys., 19, 1327–1342, https://doi.org/10.5194/acp-19-1327-2019, 2019.

Chen, L., Peng, C., Gu, W., Fu, H., Jian, X., Zhang, H., Zhang, G., Zhu, J., Wang, X., and Tang, M.: On mineral dust

aerosol hygroscopicity, Atmos. Chem. Phys., 20, 13611–13626, https://doi.org/10.5194/acp-20-13611-2020, 2020.

Covert, D. S., Charlson, R. J., and Ahlquist, N. C.: A study of the Relationship of Chemical Composition and Humidity to Light Scattering by Aerosols, J. Appl. Meteorol., 11, 968–976, https://doi.org/10.1175/1520-0450(1972)011<0968:ASOTRO>2.0.CO;2, 1972.

Dawson, K. W., Ferrare, R. A., Moore, R. H., Clayton, M. B., Thorsen, T. J., and Eloranta, E. W.: Ambient Aerosol Hygroscopic Growth From Combined Raman Lidar and HSRL, J. Geophys. Res.-Atmos., 125, e2019JD031708, https://doi.org/10.1029/2019JD031708, 2020.

Dusek, U., Frank, G. P., Hildebrandt, L., Curtius, J., Schneider, J., Walter, S., Chand, D., Drewnick, F., Hings, S., Jung, D., Borrmann, S., and Andreae, M. O.: Size Matters More Than Chemistry for Cloud-Nucleating Ability of Aerosol Particles, Science, 312, 1375–1378, https://doi.org/10.1126/science.1125261, 2006.

Düsing, S., Ansmann, A., Baars, H., Corbin, J. C., Denjean, C., Gysel-Beer, M., Müller, T., Poulain, L., Siebert, H., Spindler, G., Tuch, T., Wehner, B., and Wiedensohler, A.: Measurement report: Comparison of airborne, in situ measured, lidar-based, and modeled aerosol optical properties in the central European background – identifying sources of deviations, Atmos. Chem. Phys., 21, 16745–16773, https://doi.org/10.5194/acp-21-16745-2021, 2021.

Feingold, G. and Morley, B.: Aerosol hygroscopic properties as measured by lidar and comparison with in situ measurements, J. Geophys. Res., 108, 4327, https://doi.org/10.1029/2002JD002842, 2003.

Fernández, A. J., Apituley, A., Veselovskii, I., Suvorina, A., Henzing, J., Pujadas, M., and Artíñano, B.: Study of aerosol hygroscopic events over the Cabauw experimental site for atmospheric research (CESAR) using the multi-wavelength Raman lidar Caeli, Atmos. Environ., 120, 484–498, https://doi.org/10.1016/j.atmosenv.2015.08.079, 2015.

Foth, A., Baars, H., Di Girolamo, P., and Pospichal, B.: Water vapour profiles from Raman lidar automatically calibrated by microwave radiometer data during HOPE, Atmos. Chem. Phys., 15, 7753–7763, https://doi.org/10.5194/acp-15-7753-2015, 2015.

Gomez, S. L., Carrico, C. M., Allen, C., Lam, J., Dabli, S., Sullivan, A. P., Aiken, A. C., Rahn, T., Romonosky, D., Chylek, P., Sevanto, S., and Dubey, M. K.: Southwestern U.S. Biomass Burning Smoke Hygroscopicity: The Role of Plant Phenology, Chemical Composition, and Combustion Properties, J. Geophys. Res.-Atmos., 123, 5416–5432, https://doi.org/10.1029/2017JD028162, 2018.

Granados-Muñoz, M. J., Navas-Guzmán, F., Bravo-Aranda, J. A., Guerrero-Rascado, J. L., Lyamani, H., Valenzuela, A., Titos, G., Fernández-Gálvez, J., and Alados-Arboledas, L.: Hygroscopic growth of atmospheric aerosol particles based on active remote sensing and radiosounding measurements: selected cases in southeastern Spain, Atmos. Meas. Tech., 8, 705–718, https://doi.org/10.5194/amt-8-705-2015, 2015.

Gysel, M., Crosier, J., Topping, D. O., Whitehead, J. D., Bower, K. N., Cubison, M. J., Williams, P. I., Flynn, M. J., McFiggans, G. B., and Coe, H.: Closure study between chemical composition and hygroscopic growth of aerosol particles during TORCH2, Atmos. Chem. Phys., 7, 6131–6144, https://doi.org/10.5194/acp-7-6131-2007, 2007.

Hänel, G.: The Properties of Atmospheric Aerosol Particles as Functions of the Relative Humidity at Thermodynamic Equilibrium with the Surrounding Moist Air, Adv. Geophys., 19, 73–188, https://doi.org/10.1016/S0065-2687(08)60142-9, 1976.

Hansen, J., Sato, M., and Ruedy, R.: Radiative forcing and climate response, J. Geophys. Res., 102, 6831–6864, https://doi.org/10.1029/96JD03436, 1997.

Hu, Q., Goloub, P., and Dubovik, O.: École doctorale Sciences de la matière, N., du rayonnement et de l'environnement (Villeneuve d'Ascq, and atmosphérique (LOA), L. d'optique: Advanced Aerosol Characterization Using Sun/sky Photometer and Multi-wavelength Mie-Raman Lidar Measurements, PhD thesis, 2018.

Louf, V., Pujol, O., Sauvageot, H., and Riédi, J.: Seasonal and diurnal water vapour distribution in the Sahelian area from microwave radiometric profiling observations, Q. J. Roy. Meteor. Soc., 141, 2643–2653, https://doi.org/10.1002/qj.2550, 2015.

Navas-Guzmán, F., Martucci, G., Collaud Coen, M., Granados-Muñoz, M. J., Hervo, M., Sicard, M., and Haefele, A.: Characterization of aerosol hygroscopicity using Raman lidar measurements at the EARLINET station of Payerne, Atmos. Chem. Phys., 19, 11651–11668, https://doi.org/10.5194/acp-19-11651-2019, 2019.

Petters, M. D. and Kreidenweis, S. M.: A single parameter representation of hygroscopic growth and cloud condensation nucleus activity, Atmos. Chem. Phys., 7, 1961–1971, https://doi.org/10.5194/acp-7-1961-2007, 2007.

Sicard, M., Fortunato dos Santos Oliveira, D. C., Muñoz-Porcar, C., Gil-Díaz, C., Comerón, A., Rodríguez-Gómez, A., and Dios Otín, F.: Measurement report: Spectral and statistical analysis of aerosol hygroscopic growth from multi-wavelength lidar measurements in Barcelona, Spain, Atmos. Chem. Phys., 22, 7681–7697, https://doi.org/10.5194/acp-22-7681-2022, 2022.

Thorsen, T. J., Ferrare, R. A., Kato, S., and Winker, D. M.: Aerosol Direct Radiative Effect Sensitivity Analysis, J. Climate, 33, 6119–6139, https://doi.org/10.1175/JCLI-D-19-0669.1, 2020.

Twomey, S. and Warner, J.: Comparison of Measurements of Cloud Droplets and Cloud Nuclei, J. Atmos. Sci., 24, 702–703, 1967.

Veselovskii, I., Hu, Q., Goloub, P., Podvin, T., Korenskiy, M., Pujol, O., Dubovik, O., and Lopatin, A.: Combined use of Mie–Raman and fluorescence lidar observations for improving aerosol characterization: feasibility experiment, Atmos. Meas. Tech., 13, 6691–6701, https://doi.org/10.5194/amt-13-6691-2020, 2020.

Veselovskii, I., Hu, Q., Goloub, P., Podvin, T., Barchunov, B., and Korenskii, M.: Combining Mie–Raman and fluorescence observations: a step forward in aerosol classification with lidar technology, Atmos. Meas. Tech., 15, 4881–4900, https://doi.org/10.5194/amt-15-4881-2022, 2022.

Whiteman, D. N., Melfi, S. H., and Ferrare, R. A.: Raman lidar system for the measurement of water vapor and aerosols in the Earth's atmosphere, Appl. Optics, 31, 3068–3082, https://doi.org/10.1364/AO.31.003068, 1992.

Zieger, P., Aalto, P. P., Aaltonen, V., Äijälä, M., Backman, J., Hong, J., Komppula, M., Krejci, R., Laborde, M., Lampilahti, J., de Leeuw, G., Pfüller, A., Rosati, B., Tesche, M., Tunved, P., Väänänen, R., and Petäjä, T.: Low hygroscopic scattering enhancement of boreal aerosol and the implications for a columnar optical closure study, Atmos. Chem. Phys., 15, 7247–7267, https://doi.org/10.5194/acp-15-7247-2015, 2015.